Spatially Directed Proteomics of the Human Lens Outer Cortex Reveals an Intermediate Filament Switch Associated With the Remodeling Zone

Jamie L. Wenke, W. Hayes McDonald, and Kevin L. Schey

Vanderbilt University School of Medicine, Department of Biochemistry, Mass Spectrometry Research Center, Nashville, Tennessee, United States

Correspondence: Kevin L. Schey, Department of Biochemistry, Mass Spectrometry Research Center, PMB 407916, Vanderbilt University, Nashville, TN 37240-7916, USA; k.schey@vanderbilt.edu.

Submitted: April 22, 2016
Accepted: June 15, 2016

Citation: Wenke JL, McDonald WH, Schey KL. Spatially directed proteomics of the human lens outer cortex reveals an intermediate filament switch associated with the remodeling zone. *Invest Ophthalmol Vis Sci.* 2016;57:4108–4114. DOI:10.1167/iovs.16-19791

Purpose. To quantify protein changes in the morphologically distinct remodeling zone (RZ) and adjacent regions of the human lens outer cortex using spatially directed quantitative proteomics.

Methods. Lightly fixed human lens sections were deparaffinized and membranes labeled with fluorescent wheat germ agglutinin (WGA-TRITC). Morphology directed laser capture microdissection (LCM) was used to isolate tissue from four distinct regions of human lens outer cortex: differentiating zone (DF), RZ, transition zone (TZ), and inner cortex (IC). Liquid chromatography-tandem mass spectrometry (LC-MS/MS) of the plasma membrane fraction from three lenses (21-, 22-, and 27-year) revealed changes in major cytoskeletal proteins including vimentin, filensin, and phakinin. Peptides from proteins of interest were quantified using multiple reaction monitoring (MRM) mass spectrometry and isotopically-labeled internal peptide standards.

Results. Results revealed an intermediate filament switch from vimentin to beaded filament proteins filensin and phakinin that occurred at the RZ. Several other cytoskeletal proteins showed significant changes between regions, while most crystallins remained unchanged. Targeted proteomics provided accurate, absolute quantification of these proteins and confirmed vimentin, periplakin, and periaxin decrease from the DF to the IC, while filensin, phakinin, and brain acid soluble protein 1 (BASP1) increase significantly at the RZ.

Conclusions. Mass spectrometry-compatible fixation and morphology directed laser capture enabled proteomic analysis of narrow regions in the human lens outer cortex. Results reveal dramatic cytoskeletal protein changes associated with the RZ, suggesting that one role of these proteins is in membrane deformation and/or the establishment of ball and socket joints in the human RZ.

Keywords: ocular lens, beaded filaments, intermediate filaments, remodeling zone

Unique structural and molecular features enable the transparent ocular lens to perform its physiological function; that is, to focus light onto the retina for clear vision. Throughout life, the monolayer of lens epithelial cells differentiates into elongated lens fiber cells, which span from anterior to posterior regions of the lens.[1] Differentiating fiber cells lose all organelles and express high concentrations of lens-specific proteins including crystallins, AQP0, and beaded filament proteins: filensin and phakinin.[1–5] An equatorial cross-section view of the lens reveals hexagonally-shaped fiber cells are tightly packed in order to reduce extracellular space and thus prevent light scattering.[1] Further into the lens, fiber cells develop interdigitations that enable communication and structural stability.[1,6,7] Ball and socket joints are localized to the sides of fiber cells, while longer interlocking protrusions are at the vertices or corners of cells. Disruption of cellular packing and intracellular connections results in abnormal optical quality of the lens and lenticular haze in beaded filament protein knockout animals,[7–9] and dysregulation of interdigitations in AQP0 or beaded filament knockout animals.[10] Thus, well-regulated differentiation and fiber cell organization is critical for normal lens physiology.

Recently, a remarkable change in cell morphology was described in the human lens outer cortex in a region termed the remodeling zone (RZ).[11] Immunofluorescence microscopy images showed that the ordered differentiating human fiber cells undergo extreme morphologic changes in the narrow (~20–40 μm wide) RZ, followed by a return to classic hexagonal cell shape and organized fiber cell packing before compaction in the adult nucleus.[12] Although clear cellular outlines and radial cell columns cannot be distinguished in the RZ, it is not a barrier to diffusion and cells within the zone are nucleated, indicating they can synthesize new protein.[11,12] The remodeling zone was first characterized in human lenses and has recently been described in macaque monkey, a nonhuman primate.[13] Transmission electron microscopy (TEM) images revealed irregular cell shape and numerous ball-and-socket joints originating in the RZ.[12] This zone is visible and is reproducible in size and distance from the capsule across a wide age range of human lenses, suggesting the RZ is a regulated process of differentiation in primate lenses.[11,12] The

Investigative Ophthalmology & Visual Science

function and molecular changes associated with the primate-specific RZ remain to be characterized.

The purpose of this study was to characterize the membrane-associated proteome of the RZ and adjacent regions. Because the narrow RZ is located ~ 100 μm beneath the lens capsule and is approximately 20 to 40 μm wide, we used laser capture microdissection (LCM) to collect tissue for spatially resolved proteomics. We implemented a mass spectrometry-compatible fixation protocol that preserved the morphology of the lens outer cortex. Four regions were isolated for analysis: differentiating zone (DF), RZ, transition zone (TZ), and inner cortex (IC). Shotgun proteomics revealed initial candidates for subsequent targeted protein quantification, and heavy-labeled peptides were synthesized as internal standards for multiple reaction monitoring (MRM) proteomics experiments. Our results highlighted a change in abundance from the intermediate filament (IF) protein vimentin to beaded filament proteins filensin and phakinin at the RZ, and significant abundance changes in other cytoskeletal proteins in these regions.

Experimental Methods

Materials

Proteomics-grade porcine trypsin, ethanol, high-performance liquid chromatography (HPLC)-grade acetonitrile, formic acid, urea, phosphate buffered saline (PBS), sodium hydroxide, tris(hydroxymethyl)aminomethane (Tris), and xylenes were purchased from Sigma-Aldrich Corp. (St. Louis, MO, USA). Acetic acid, ammonium bicarbonate, dithiothreitol (DTT), chloroacetamide (ClAA), HPLC-grade H_2O with 0.1% formic acid, HPLC-grade H_2O, and HPLC-grade acetonitrile with 0.1% formic acid were from Fisher Scientific (Pittsburgh, PA, USA). 2,2,2-Trifluoroethanol (TFE) was purchased from Acros Organics.

Fresh human lenses were obtained from the National Disease Research Interchange (Philadelphia, PA, USA). Lenses used in this study were from individuals with no reported ocular pathology. Three lenses were analyzed in total: 21-year (M), 22-year (M), and 27-year (F). All other reagents were purchased from Sigma-Aldrich Corp. unless otherwise stated.

Sample Preparation and LCM

Lenses were stored on wet ice during shipment and fixed immediately upon arrival. A solution of 75:25 ethanol:acetic acid was used to lightly fix tissue while avoiding traditional formaldehyde crosslinking that can interfere with mass spectrometry experiments.[14] Whole lenses were fixed for 12 hours, manually cut in half across the equator using a razor blade, and fixed for an additional 12 hours. After fixation, lenses were processed and embedded in paraffin. Eight micron sections were cut and collected using a Microm HM 325 Microtome (Thermo Scientific, Waltham, MA, USA) and allowed to dry on glass slides overnight at 37°C. Sections were deparaffinized prior to labeling, using a series of xylene and alcohol washes (xylenes × 3, 100% ethanol, 95% ethanol, 70% ethanol, PBS – 5 minutes each).

To visualize the RZ, lenses were incubated in wheat germ agglutinin-TRITC (Life Technologies, Eugene, OR, USA), using a 1 mg/mL stock solution at 1:100 dilution for 2 hours, followed by three, 5-minute PBS washes. Sections for LCM were coverslipped until dry to maintain a flat section. Coverslips were removed prior to tissue capture. Sections used for confocal imaging were covered with VECTASHIELD mounting medium (Vector Laboratories, Burlingame, CA, USA) and sealed with a coverslip. Nuclei were labeled with 4′,6-diamidino-2-phenylindole (DAPI).

Laser capture microdissection was performed on a PALM MicroBeam system (Carl Zeiss Microscopy, Thornwood, NY, USA). Uncovered sections were visualized at 20× magnification using the rhodamine fluorescence setting (540/600 nm excitation/emission). Regions of interest were manually selected in the software, based on cellular morphology and measured distance from lens capsule. Tissue was cut in brightfield mode and cells from each selected region were catapulted into an Eppendorf cap containing 25-μL HPLC-grade H_2O. Microdissection was carried out until 2×10^6 μm^2 tissue was collected for each region to ensure approximately equal starting material. In total, tissue from four regions was collected: DF (outer fiber cell layers, 0–100 μm from lens capsule); RZ (100–140 μm from lens capsule); TZ (140–240 μm from lens capsule); IC (240 μm and beyond). Tissue was then spun down into the tube and frozen for side-by-side membrane preparation of all four regions. For each lens, a total of three replicates of DF, RZ, TZ, and IC were collected for initial experiments. Three lenses were analyzed in total (21-, 22-, and 27-year).

Membrane Preparation and Shotgun Proteomics

Collected cells were washed to prepare membranes and to remove soluble proteins, as described previously.[15] Samples were first reduced (25 mM DTT, 56°C for 1 hour) and alkylated (55 mM ClAA, room temperature, 45 minutes in dark) before a series of washing and centrifugation steps to remove soluble proteins. The sample was vortexed and incubated for 30 minutes in homogenizing buffer containing 8 M urea (50 mM ammonium bicarbonate, 5 mM EDTA, 10 mM NaF, 1 mM DTT, pH 8), followed by 20-minute centrifugation at 100,000*g* (Sorvall MTX150 Micro Ultracentrifuge, Thermo Scientific). The supernatant was removed and the pellet was saved and washed further using the following procedure: homogenizing buffer containing 8 M urea (three times total), 0.1M NaOH (one time), HPLC-grade H_2O (one time), 95% ethanol (one time), and HPLC-grade H_2O (three times). Prior to trypsin digestion, the pellet was resuspended in 50% TFE in 50 mM ammonium bicarbonate, then diluted to 5% TFE before addition of 1 μL of 0.1 μg/μL trypsin (Pierce) in a volume of 100 μL. Digestion proceeded overnight at 37°C and was stopped with the addition of 0.2 μL neat formic acid.

For each tissue region, the entire sample was bomb-loaded onto a reverse-phase 360 μm outer diameter (o.d.) × 100 μm inner diameter (i.d.) capillary trap column (3 cm length/5 μm Jupiter C_{18} beads, 300 Å, Phenomenex) in-line with a 360 μm o.d. × 100 μm i.d. reverse-phase analytical column packed with 20 cm Jupiter C_{18} beads (3 μm, 300 Å, Phenomenex) and equipped with a laser-pulled emitter tip. Using an Eksigent nanoLC-ultra HPLC system, peptides were eluted at a flow rate of 500 nL/min over a 120-minute gradient of 0.1% formic acid in water (solvent A) and 0.1% formic acid in acetonitrile (solvent B). The gradient consisted of 2% to 10% B in 20 minutes, 10% to 30% B in 30 minutes, 30% to 95% B in 15 minutes, 95% B for 15 minutes, followed by equilibration at 2% B. Gradient-eluted peptides were mass analyzed on an LTQ Velos Pro linear ion trap mass spectrometer with a nano-electrospray ionization source (Thermo Scientific). The instrument was operated using a data-dependent method with dynamic exclusion enabled. Full scan (*m/z* 300–2000) spectra were acquired and the top 10 most abundant ions in each MS scan were selected for fragmentation via collision-induced dissociation (CID). Tandem mass spectra were converted into DTA files using Scansifter[16] and searched using a custom version of Sequest (Thermo Fisher Scientific)[17] operating on the Vanderbilt ACCRE computing cluster. Tandem mass (MS/

MS) spectra were searched against a concatenated forward and reverse (decoy) database containing the *Homo sapiens* subset of UniprotKB Sprot protein database (www.uniprot.org in the public domain). Additional search parameters included: trypsin enzyme specificity, monoisotopic masses were used for searching product ions, and oxidation of methionine, carbamidomethylation of cysteine, and phosphorylation of serine, threonine and tyrosine were allowed as variable modifications. Scaffold 4.3.4 (Proteome Software, Portland, OR, USA) was used to summarize and validate search results, where a minimum probability threshold of 95% was required for peptide identifications and data were filtered to a false-discovery rate (FDR) of $< 1\%$ at the protein level. Peptide abundance in each region was compared using normalized spectral counts and a Student's *t*-test was used to determine whether differences between the DF and RZ were statistically significant ($P < 0.05$).

Quantitative MRM

Proteins with statistically significant changes near the RZ were selected for further quantitation using MRM.[18] Representative peptides for each protein were selected based on their appearance across multiple samples in the discovery phase of analysis described above. Heavy-labeled peptide standards were synthesized by jpt (SpikeTides TQL peptides, jpt, Berlin, Germany). Peptides contained isotopically labeled terminal arginine or lysine residues (^{13}C and ^{15}N) and a trypsin-cleavable C-terminal tag. Peptide standards were used to generate a calibration curve, which confirmed a linear response between 1.5 and 100 fmol/μL (data not shown). After membrane enrichment and before enzymatic digestion, isotopically labeled peptides were spiked into samples at approximately endogenous levels. Skyline software (University of Washington, MacCoss lab)[19] was used to set up scheduled, targeted MRM methods and four to five MS/MS transitions were monitored per peptide. For targeted proteomics, 6×10^6 μm^2 tissue was collected and membranes were prepared as described above. Prior to trypsin digestion, the pellet was resuspended in 8 M urea (100 mM Tris buffer, pH 8), then diluted with 100 mM Tris to 2 M urea before addition of 1 μL of 0.1 μg/μL trypsin (mass spectrometry-grade, Pierce) in a total volume of 10 μL. Digestion proceeded overnight at 37°C and was stopped with the addition of a small amount of neat formic acid.

The 10 μL digest was transferred to a reduced-volume autosampler vial and 2.5 μL sample per run was injected via autosampler (NanoAcuity HPLC system, Waters) onto a vented column setup[20] utilizing a 40 mm by 0.1 mm (Jupiter 5 micron, 300A) kasil fritted trap followed by a 200 mm by 0.1 mm (Jupiter 3 micron, 300A), self-packed analytical column coupled directly to a TSQ-Vantage (Thermo Scientific) via a nanoelectrospray source. After trapping and equilibration, peptides were resolved using a 90-minute aqueous to organic gradient (solvent A = 0.1% FA in water and B = 0.1% FA in ACN) operating at 400 nL/min. A series of unscheduled runs determined retention times and the most useful transitions to monitor and then a scheduled instrument method encompassing a 6-minute window around the measured retention time along with calculated collision energies was created using Skyline. Q1 peak width resolution was set to 0.7, collision gas pressure was 1 mTorr, and utilized an EZ method cycle time of 3 seconds. The resulting RAW instrument files were imported into Skyline for peak-picking and quantitation. Transition or fragment ion peak areas were summed to represent the intensity of endogenous peptides, which were normalized to the internal standard. For statistical analysis, a 1-way ANOVA was performed with a post hoc multiple comparison Tukey test using SPSS software (IBM, Armonk, New York, USA).

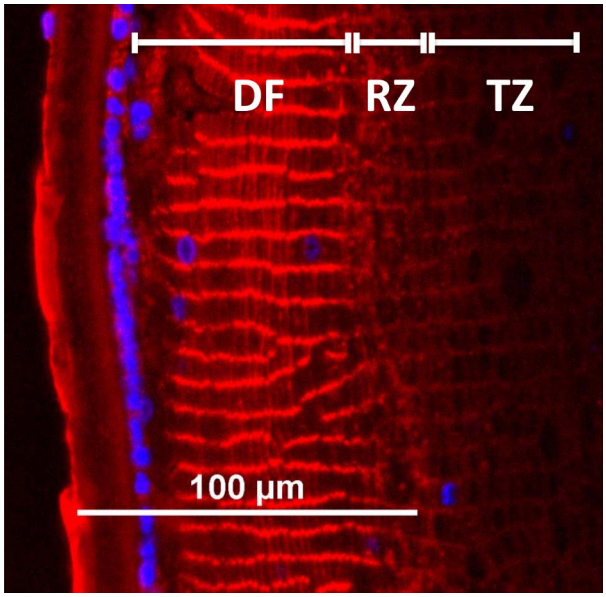

FIGURE 1. Confocal microscopy image of 22-year human lens. Lens was ethanol-fixed and sectioned, followed by labeling with WGA-TRITC to highlight cell membranes. Nuclei were labeled with DAPI. The ordered differentiating fiber cells (DF) rapidly become morphologically more complex in the RZ before radial cell columns are again visible in the TZ.

RESULTS

Lens Fixation for LCM and Liquid Chromatography-Tandem Mass Spectrometry (LC-MS/MS)

Although traditional fixation enables excellent antibody and lectin labeling of lens fiber cells, it causes protein-protein crosslinking that can interfere with traditional mass spectrometry proteomic analysis that uses trypsin to cleave at basic residues.[14] Thus, we attempted alternative mass spectrometry-compatible fixation methods that could preserve cellular structure, including the lens capsule and outer cell layers. Fresh human lenses were lightly fixed in 75:25 ethanol:acetic acid for a total of 24 hours. Wheat germ agglutinin-labeled paraffin sections showed the outer cell layers remained intact and cellular morphology could be visualized. Confocal fluorescence microscopy images confirmed the presence of the RZ approximately 100 μm beneath the lens capsule (Fig. 1). A return to more ordered cellular organization is visible in the TZ (140–240 μm from lens capsule) where cellular compaction begins. A test section was processed and analyzed by LC-MS/MS to ensure this fixation did not interfere with trypsin digestion and mass spectrometry (data not shown).

Shotgun Proteomics

After light fixation and WGA labeling, lens sections were visualized on the LCM instrument using the fluorescence microscope setting. Regions of interest (shown in Fig. 1) were manually selected based on membrane morphology and distance from the capsule. Regions and approximate measurements included differentiating fiber cells (DF, outer fiber cell layers, 0–100 μm from lens capsule); RZ (100–140 μm from lens capsule); TZ (140–240 μm from lens capsule); IC (240 μm and beyond); 2×10^6 μm^2 of tissue was collected per region, which is equivalent to approximately 80,000 fiber cell cross-sections based on average fiber cell diameter.[21] After each

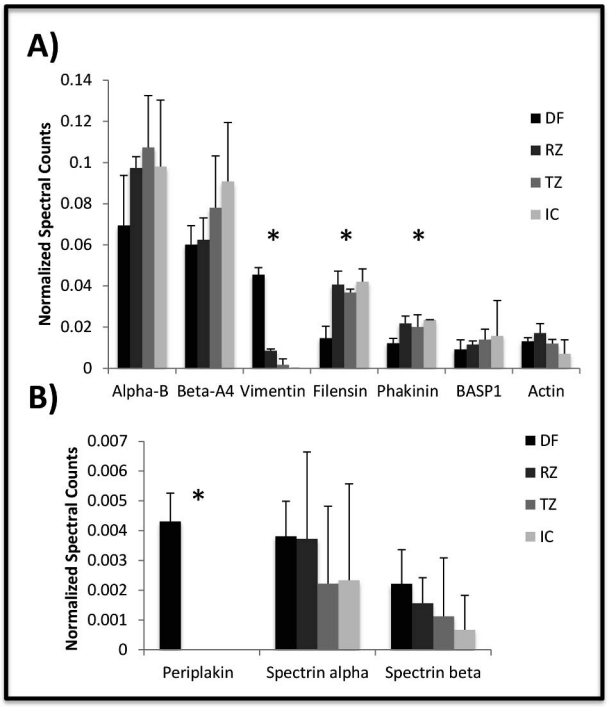

FIGURE 2. Shotgun proteomics results from a 22-year human lens. Three LC-MS/MS runs were averaged for each region. * Indicates a statistically significant difference detected between the DF and RZ regions ($P < 0.05$).

sample was prepared to isolate integral membrane and membrane-associated proteins, the proteins were digested with trypsin and were analyzed by LC-MS/MS. Shotgun proteomics results identified expected lens proteins, ranging from crystallins to cytoskeletal proteins (full protein list for 22y lens in Supplementary Table S1). Compared to conventional tissue homogenization proteomics experiments, total spectral counts from our LCM samples are quite low due to the very small amount of tissue captured and prepared for proteomic analysis. The small amount of tissue is also likely why naturally abundant lens fiber major intrinsic protein (AQP0) only appears in the RZ region at low spectral counts given that trypsin efficiency is likely low for this integral membrane protein.

To identify proteins that were changing in the RZ, we initially performed the Student's *t*-test to compare peptide spectral counts between the DF and RZ regions. Statistically significant changes were detected for the IF protein vimentin, which decreases by approximately 80% from the DF to the RZ (Fig. 2) and decreases further in the TZ and IC. A concurrent increase in the beaded filament proteins filensin and phakinin is observed at the RZ, suggesting a switch of IFs occurs near the RZ. Other cytoskeletal proteins including periplakin also change significantly, while spectrins and several crystallins remained fairly constant across the regions analyzed. These results were used to develop a targeted quantitative mass spectrometry assay for more accurate quantitation of proteins of interest with significant changes at the RZ.

Quantitative MRM

To more accurately quantify protein changes around the RZ, we adopted a targeted proteomics strategy, using MRM for protein quantitation. In this experiment, known concentrations of heavy-labeled isotopes for each peptide of interest that

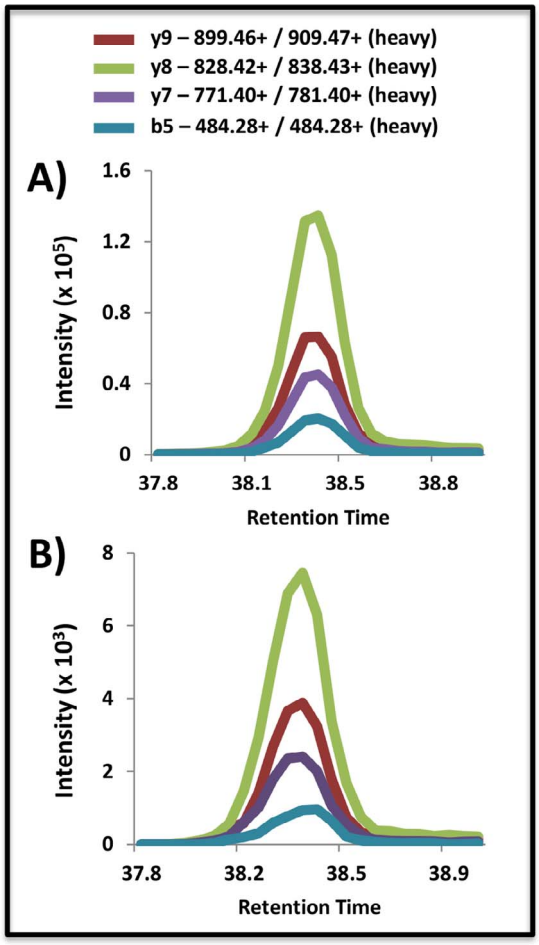

FIGURE 3. Transitions, or peptide fragmentation patterns, selected for MRM of a filensin tryptic peptide ($_{77}$LGELAGPEDALAR$_{89}$). Precursor masses for endogenous (*m/z* 656.35, +2) and heavy (*m/z* 661.35, +2) peptides were monitored along with characteristic fragment transitions shown above. Relative intensity and retention time of heavy peptide standard transitions (**A**) are consistent with endogenous peptide (**B**).

differ in mass from the endogenous peptide but share physiochemical properties and behave similarly in the instrument were spiked into samples. Absolute endogenous peptide concentrations can be calculated from the measured ratio of the endogenous peptide to its heavy-labeled counterpart and the known concentration of the heavy internal standard.

Using shotgun proteomics data, one to three representative peptides were chosen for each protein of interest (Supplementary Table S2). Peptides were selected based on several criteria, including identification across several mass spectrometry runs and biological samples, absence of labile or modifiable residues like methionine or cysteine, and ideal peptide length (~7–20 amino acids) for detection by mass spectrometry. Standard curves were measured to determine the quantifiable range of the internal standards (data not shown) and the concentration of each internal peptide standard was optimized to approximate endogenous peptide levels. For the final analysis, the 4 regions of interest were isolated from 3 separate lenses (21-, 22-, and 27-year). A larger amount of tissue (6×10^6 μm^2) was pooled for each region so technical replicates could be run for each sample. An example of the MRM signals observed for an endogenous and heavy-labeled filensin peptide is shown in Figure 3.

Targeted, quantitative MRM results generally agreed with shotgun proteomics results, providing more confidence and better quantitation of small abundance changes between the four regions. Figure 4 shows the relative intensity of peptides quantified from 3 different lenses (two technical replicates per lens). Intensities are normalized to the region with the highest peptide concentration; other regions are expressed as a percentage of the highest value. Statistically significant changes were determined using a 1-way ANOVA with Tukey test independently for each peptide. Both vimentin peptides decreased 80% from the DF to the RZ, in agreement with shotgun proteomics data, and continued to decrease in the TZ and IC (Fig. 4A). Periplakin and periaxin follow similar trends, decreasing by 30% to 40% from DF to RZ and even further in the TZ (Figs. 4B, 4C). Filensin and phakinin, which make up the beaded filament of the lens, increase at least 2-fold at the RZ and show slightly variable but decreasing abundance in the TZ with a trend toward increasing abundance in the IC (Figs. 4E, 4F). In Figure 4D, brain acid soluble protein 1 (BASP1) follows a similar trend where increasing abundance was observed at the RZ compared to the DF zone with slightly less protein detected in the TZ and IC. Supplementary Table S3 shows the absolute quantitation of peptides in each region from three separate lenses, where peptide abundances (fmol) calculated represent the peptide quantity in approximately 2×10^6 μm^2 tissue collected. Despite some discrepancies in the absolute fmol calculated per lens, which could be due to differences in tissue thickness, the trends match very well among the three ages studied. Differences in the absolute amount of peptides from the same protein could be due to differing digestion efficiency, ionization efficiency, peptide solubility, or the presence of posttranslational modifications that affect peptide m/z and therefore signal for targeted peptide analysis. These issues may be particularly relevant for membrane and cytoskeletal proteins.

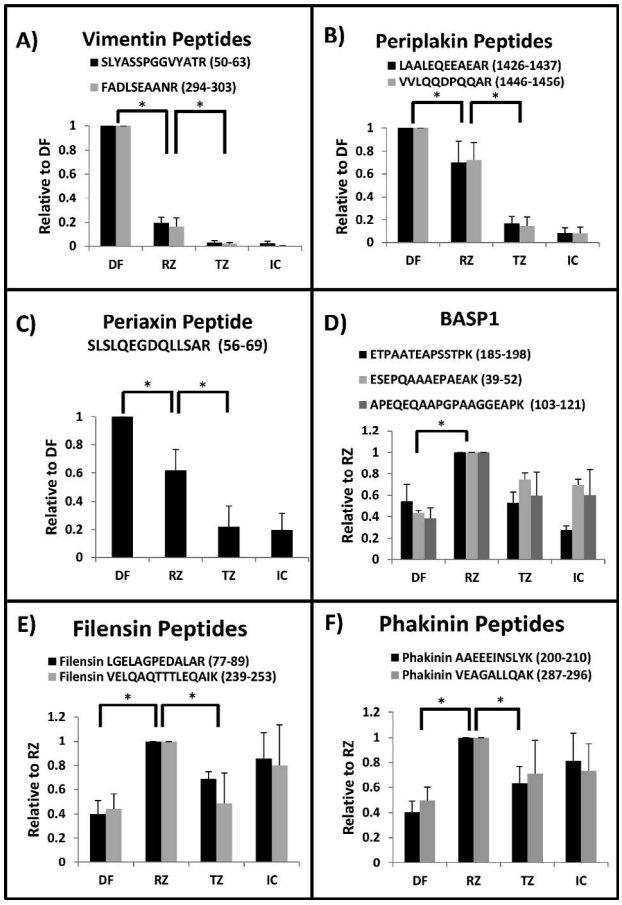

FIGURE 4. Quantitative proteomics of selected lens proteins. Each bar represents six measurements (two technical replicates per lens, three lenses total: 21-, 22-, and 27-year). After calculating fmol values for each representative peptide, the region with the highest signal was set to "1" and other regions expressed as a fraction of that value. A 1-way ANOVA with Tukey test was used to determine statistically significant differences between regions. Brackets with (*) indicate $P < 0.05$.

DISCUSSION

Several different methods have been used to study changes in membrane-associated proteins in different lens fiber cell populations. After gross dissection of whole human lenses, the quantitative proteomics method of iTRAQ was used to assess binding of cytosolic proteins to the plasma membrane with age.[22] The combination of LCM and LC-MS/MS has also been used previously to analyze differences in the bovine cortical and nuclear lens membrane proteome.[15] Here, we isolated extremely narrow regions (20–30 μm) of tissue for quantitative proteomic analysis of the human lens outer cortex to determine molecular changes associated with the extreme morphologic changes of the plasma membrane in the RZ.[11,12] These techniques enable spatially resolved proteomics of regions that cannot be separated by manual dissection. Although we enriched for the plasma membrane fraction, the majority of proteins detected by proteomic analysis were crystallins and cytoskeletal proteins, likely due to their high abundance and reported association with the plasma membrane, even after treatment with urea.[4,23–25] Based on these results, we could not assess membrane protein changes and instead focused on cytoskeletal proteins. Targeted proteomics analysis enabled relative quantitation of peptides between different lens regions, even those present at low levels.

Intermediate filaments are a highly conserved family of cytoskeletal proteins that can be organized into several classes.[26] Immunohistochemical studies indicate vimentin, a major type III IF protein, is expressed in the lens epithelium and fiber cells, although the expression pattern changes based on lens age and region.[4,27,28] Our results indicate vimentin is most abundant in the very outer fiber cells of the DF region and its abundance decreases in the RZ and further into the lens. Because we analyzed the plasma membrane fraction, this decrease in vimentin signal at the RZ could be due to either reduced vimentin expression, increased solubility of the protein, or decreased association with the plasma membrane. It is possible that loss of vimentin in the RZ is due to a shift from membrane to cytoplasm, which has been documented in the literature.[27] Studies of adult mouse lens show membrane-specific vimentin localization in outer cortical fibers, while vimentin antibody labeling is both cytoplasmic and membranous further into the lens before signal is lost around the region of nuclei loss.[27] Similar labeling patterns have also been documented in bovine lens.[29] Furthermore, loss of vimentin antibody labeling has been correlated with nuclei loss in mouse lens.[27] However, we observe a decrease in vimentin signal in the RZ, before nuclei are completely lost. It is possible that the drop in vimentin signal in our experiments could be due to changes in vimentin solubility or membrane association.[30] Deeper into the lens cortex, vimentin is known to be cleaved, which could affect solubility and detection by both immunohistochemistry and mass spectrometry. Phosphorylation of vimentin is known to induce depolymerization of IFs, although this modification was not detected in our studies. Although vimentin knockout does not result in any notable

phenotype, vimentin overexpression causes cataract, suggesting that proper expression and regulation of vimentin is critical for lens clarity.[31–33]

The lens contains another divergent IF called the beaded filament. Filensin and phakinin are lens-specific proteins that assemble to make 6 to 8 nm beaded filaments.[4] Our results indicate that filensin and phakinin levels increase significantly from the DF to the RZ, while vimentin decreases. The switch from vimentin IFs to lens-specific beaded filaments containing filensin and phakinin has been documented in several species including bovine and mouse.[29,34] The control of these two IF systems appears to be independently modulated during fiber cell differentiation, as beaded filament expression is detected before vimentin labeling is lost.[29] Adult mouse lenses labeled with anti-filensin antibody reveal membraneous labeling in the outer cortex, followed by membranous and cytoplasmic labeling further into the nucleated lens fiber cells.[27] However, filensin is not present in developing embryonic fiber cells until after elongation has progressed, suggesting it plays a role in lens organization after cells have begun differentiation.[27] Filensin and phakinin have also been shown to undergo truncation deeper into the lens.[35] The decrease in signal from RZ to TZ could be due to several factors, including altered solubility or membrane association. The functional consequences of beaded filament increase in the RZ have not been established. However, TEM studies indicate ball and socket joints arise in the RZ,[12] and knockout studies indicate beaded filaments are critical for maintaining interdigitations and long-range order of lens fiber cells.[34] Therefore, filensin and phakinin may become more associated with the membrane to establish interlocking domains and a beaded filament system that is maintained further into the lens cortex. The switch from IFs to beaded filaments at the RZ suggests an important role for lens-specific IFs.

Periaxin and periplakin decrease from the RZ to the IC, similar to vimentin. Periaxin is localized to the plasma membrane, concentrated mostly at tricellular junctions where beaded filaments and vimentin labeling also occur.[36] Periaxin is critical for hexagonal geometry and membrane stabilization, perhaps functioning as a scaffolding protein in lens.[36] Periplakin, an IF-associated protein (IFAP), has been shown to bind both IFs and beaded filaments, directly interacting with vimentin and phakinin.[37] Periplakin and periaxin are also part of the EPPD (ezrin, periaxin, periplakin, desmoyokin) junction complex in lens.[38] Although their roles are not well understood, both periaxin and periplakin could anchor IFs to the plasma membrane through protein-protein interactions. AQP0 has been demonstrated to interact with beaded filaments, but AQP0 did not pull down with periplakin-BF complexes in previous studies, suggesting there may be another protein anchor connecting periplakin and BF to the plasma membrane.[37] Brain acid soluble protein 1 has been detected in lens but little is known about its function in this tissue.[39] In the brain, the growth-associated protein BASP1 is localized to the plasma membrane at the tip of elongating axons.[40] Although the role of BASP1 in lens has not been established, the increase in BASP1 levels at the RZ is not surprising given its function in regulating the actin cytoskeleton in brain.[40]

Changes in protein-protein interaction, that is, between periplakin and vimentin, could alter IF attachment to the plasma membrane, serving as a way to modulate the lens cytoskeleton and thus influence membrane shape in the RZ. Actin polymerization could also be driving the formation of cellular interdigitations that originate in the RZ, as branching F-actin and the clathrin/AP-2 complex were shown to associate with interlocking domains in rat and monkey lenses.[41] Although we do not detect major changes in actin or clathrin abundance in our studies, their involvement in RZ morphology cannot be ruled out. It is possible that changes in actin polymerization or interactions with other proteins, in addition to BASP1, are important but remain undetected in our quantitative proteomics studies. Additional work is required to understand how these proteins might be involved in membrane reorganization in the RZ.

Although the switch from vimentin to beaded filaments has been documented in lens, this work is the first to show a rapid IF change associated with the human lens RZ. Our proteomics results do not definitively prove that the IF switch is responsible for the morphologic changes of the RZ, but suggest the involvement of beaded filaments in establishing the ball and socket joints that originate in the RZ.[12] This notion is supported by the loss of flap structures and long-range fiber cell stacking in the deep cortex of beaded filament knockout mice.[34] Intermediate filaments can serve as mechanical support and scaffolding for membrane-associated proteins. Changes to the IF system could allow remodeling of the plasma membrane before the fiber cells return to a more ordered arrangement in the TZ.

The function of the RZ remains to be determined. This phenomenon has only been observed in human and macaque lenses,[13] suggesting that accommodation in long-lived primates could require more extensive preparation of interdigitations between lens fiber cells. Future work should examine human lenses with cataract-causing mutations in beaded filament genes to determine whether the formation of the RZ is affected.

Conclusions

Using spatially resolved proteomics, we characterized protein changes in the narrow RZ and surrounding regions of the human lens outer cortex. Membrane-associated IFs switch from vimentin to beaded filaments in this region, with changes in other IFAPs, suggesting involvement of the cytoskeleton and associated proteins in the dramatic membrane remodeling in the RZ. Consistent quantitative results between three separate lenses suggest the RZ region is part of a tightly-regulated differentiation process in human lens. Future work is necessary to characterize the function and necessity of the RZ for normal human lens physiology.

Acknowledgments

We acknowledge support from the Proteomics Core of the Vanderbilt Mass Spectrometry Research Center.

Supported by National Institutes of Health (Bethesda, MD, USA) Grants T32-EY07135, EY-13462, P30-EY08126, 2U42OD011158.

Disclosure: **J.L. Wenke**, None; **W.H. McDonald**, None; **K.L. Schey**, None

References

1. Mathias RT, Rae JL, Baldo GJ. Physiological properties of the normal lens. *Physiol Rev*. 1997;77:21–50.
2. Wride MA. Lens fibre cell differentiation and organelle loss: many paths lead to clarity. *Philos Trans R Soc Lond B Biol Sci*. 2011;366:1219–1233.
3. Bassnett S. Lens organelle degradation. *Exp Eye Res*. 2002;74:1–6.
4. FitzGerald PG. Lens intermediate filaments. *Exp Eye Res*. 2009;88:165–172.
5. Schey KL, Wang Z, Wenke JL, Qi Y. Aquaporins in the eye: expression, function, and roles in ocular disease. *Biochim Biophys Acta*. 2014;1840:1513–1523.
6. Zampighi G, Simon SA, Robertson JD, McIntosh TJ, Costello MJ. On the structural organization of isolated bovine lens fiber junctions. *J Cell Biol*. 1982;93:175–189.

7. Sandilands A, Prescott AR, Wegener A, et al. Knockout of the intermediate filament protein CP49 destabilises the lens fibre cell cytoskeleton and decreases lens optical quality, but does not induce cataract. *Exp Eye Res*. 2003;76:385–391.
8. Alizadeh A, Clark J, Seeberger T, Hess J, Blankenship T, FitzGerald PG. Targeted deletion of the lens fiber cell-specific intermediate filament protein filensin. *Invest Ophthalmol Vis Sci*. 2003;44:5252–5258.
9. Alizadeh A, Clark JI, Seeberger T, et al. Targeted genomic deletion of the lens-specific intermediate filament protein CP49. *Invest Ophthalmol Vis Sci*. 2002;43:3722–3727.
10. Lo WK, Biswas SK, Brako L, Shiels A, Gu S, Jiang JX. Aquaporin-0 targets interlocking domains to control the integrity and transparency of the eye lens. *Invest Ophthalmol Vis Sci*. 2014;55:1202–1212.
11. Lim JC, Walker KL, Sherwin T, Schey KL, Donaldson PJ. Confocal microscopy reveals zones of membrane remodeling in the outer cortex of the human lens. *Invest Ophthalmol Vis Sci*. 2009;50:4304–4310.
12. Costello MJ, Mohamed A, Gilliland KO, Fowler WC, Johnsen S. Ultrastructural analysis of the human lens fiber cell remodeling zone and the initiation of cellular compaction. *Exp Eye Res*. 2013;116:411–418.
13. Costello MJ, Mohamed A, Gilliland KO, Wenke JL, Schey KL. *Quantitative Morphology of the Remodeling Zone in Non-Human Primate Lenses*. Poster presented at the annual Association for Research in Vision and Ophthalmology Conference. Denver, CO. 2015.
14. Sompuram SR, Vani K, Messana E, Bogen SA. A molecular mechanism of formalin fixation and antigen retrieval. *Am J Clin Pathol*. 2004;121:190–199.
15. Wang Z, Han J, Schey KL. Spatial differences in an integral membrane proteome detected in laser capture microdissected samples. *J Proteome Res*. 2008;7:2696–2702.
16. Ma ZQ, Tabb DL, Burden J, et al. Supporting tool suite for production proteomics. *Bioinformatics*. 2011;27:3214–3215.
17. Eng JK, McCormack AL, Yates JR. An approach to correlate tandem mass spectral data of peptides with amino acid sequences in a protein database. *J Am Soc Mass Spectrom*. 1994;5:976–989.
18. Gerber SA, Rush J, Stemman O, Kirschner MW, Gygi SP. Absolute quantification of proteins and phosphoproteins from cell lysates by tandem MS. *Proc Natl Acad Sci U S A*. 2003;100:6940–6945.
19. MacLean B, Tomazela DM, Shulman N, et al. Skyline: an open source document editor for creating and analyzing targeted proteomics experiments. *Bioinformatics*. 2010;26:966–968.
20. Licklider LJ, Thoreen CC, Peng J, Gygi SP. Automation of nanoscale microcapillary liquid chromatography-tandem mass spectrometry with a vented column. *Anal Chem*. 2002;74:3076–3083.
21. Taylor VL, al-Ghoul KJ, Lane CW, Davis VA, Kuszak JR, Costello MJ. Morphology of the normal human lens. *Invest Ophthalmol Vis Sci*. 1996;37:1396–1410.
22. Truscott RJ, Comte-Walters S, Ablonczy Z, et al. Tight binding of proteins to membranes from older human cells. *Age (Dordr)*. 2011;33:543–554.
23. Su SP, McArthur JD, Friedrich MG, Truscott RJ, Aquilina JA. Understanding the alpha-crystallin cell membrane conjunction. *Mol Vis*. 2011;17:2798–2807.
24. Friedrich MG, Truscott RJ. Membrane association of proteins in the aging human lens: profound changes take place in the fifth decade of life. *Invest Ophthalmol Vis Sci*. 2009;50:4786–4793.
25. Wang Z, Han J, David LL, Schey KL. Proteomics and phosphoproteomics analysis of human lens fiber cell membranes. *Invest Ophthalmol Vis Sci*. 2013;54:1135–1143.
26. Steinert PM, Roop DR. Molecular and cellular biology of intermediate filaments. *Annu Rev Biochem*. 1988;57:593–625.
27. Blankenship TN, Hess JF, FitzGerald PG. Development- and differentiation-dependent reorganization of intermediate filaments in fiber cells. *Invest Ophthalmol Vis Sci*. 2001;42:735–742.
28. Fleschner CR. Lens membrane fraction associated intermediate filaments of different aged rats. *Curr Eye Res*. 2002;24:296–304.
29. Sandilands A, Prescott AR, Carter JM, et al. Vimentin and CP49/filensin form distinct networks in the lens which are independently modulated during lens fibre cell differentiation. *J Cell Sci*. 1995;108:1397–1406.
30. Alizadeh A, Clark J, Seeberger T, Hess J, Blankenship T, FitzGerald PG. Characterization of a mutation in the lens-specific CP49 in the 129 strain of mouse. *Invest Ophthalmol Vis Sci*. 2004;45:884–891.
31. Colucci-Guyon E, Portier MM, Dunia I, Paulin D, Pournin S, Babinet C. Mice lacking vimentin develop and reproduce without an obvious phenotype. *Cell*. 1994;79:679–694.
32. Capetanaki Y, Smith S, Heath JP. Overexpression of the vimentin gene in transgenic mice inhibits normal lens cell differentiation. *J Cell Biol*. 1989;109:1653–1664.
33. Bloemendal H, Raats JM, Pieper FR, Benedetti EL, Dunia I. Transgenic mice carrying chimeric or mutated type III intermediate filament (IF) genes. *Cell Mol Life Sci*. 1997;53:1–12.
34. Yoon KH, Blankenship T, Shibata B, Fitzgerald PG. Resisting the effects of aging: a function for the fiber cell beaded filament. *Invest Ophthalmol Vis Sci*. 2008;49:1030–1036.
35. Wang Z, Obidike JE, Schey KL. Posttranslational modifications of the bovine lens beaded filament proteins filensin and CP49. *Invest Ophthalmol Vis Sci*. 2010;51:1565–1574.
36. Maddala R, Skiba NP, Lalane RR, Sherman DL, Brophy PJ, Rao PV. Periaxin is required for hexagonal geometry and membrane organization of mature lens fibers. *Dev Biol*. 2011;357:179–190.
37. Yoon KH, FitzGerald PG. Periplakin interactions with lens intermediate and beaded filaments. *Invest Ophthalmol Vis Sci*. 2009;50:1283–1289.
38. Straub BK, Boda J, Kuhn C, et al. A novel cell-cell junction system: the cortex adhaerens mosaic of lens fiber cells. *J Cell Sci*. 2003;116:4985–4995.
39. Bagchi M, Kousis S, Maisel H. BASP1 in the lens. *J Cell Biochem*. 2008;105:699–702.
40. Frey D, Laux T, Xu L, Schneider C, Caroni P. Shared and unique roles of CAP23 and GAP43 in actin regulation, neurite outgrowth, and anatomical plasticity. *J Cell Biol*. 2000;149:1443–1454.
41. Zhou CJ, Lo WK. Association of clathrin, AP-2 adaptor and actin cytoskeleton with developing interlocking membrane domains of lens fibre cells. *Exp Eye Res*. 2003;77:423–432.

Investigative Ophthalmology & Visual Science